

INTERACTION OF LASER RADIATION WITH MATTER. LASER PLASMA DOI: 10.1070/QEL15958

X-ray generation by fast electrons propagating in nanofibres irradiated by a laser pulse of relativistic intensity

A.A. Andreev, K.Yu. Platonov

Abstract. **Numerical simulations were made of the interaction of a relativistically intense laser pulse with a target consisting of nanometre fibres. Fast electrons were shown to execute forced betatron oscillations in the electrostatic fibre field and the laser field. The fibre diameter was determined whereby the amplitude of betatron electron oscillations is resonantly increased. The power of coherent X-ray betatron radiation of the electron bunch was calculated outside of the resonance domain and in the resonance case. We showed that the laser-to-X-ray betatron radiation conversion coefficient in the resonance case amounts to a few percent and the target made up of nanometre fibres may be regarded as an efficient laser-driven source of coherent X- and gamma-ray radiation.**

Keywords: *laser-driven electron acceleration, betatron radiation, nanofibres, laser-driven coherent X-ray source.*

1. Introduction

The generation of relativistic electron beams (REBs) and hard X-ray photons in the interaction of laser radiation with different targets is being intensively studied today [1]. These investigations are aimed at increasing the intensity, degrees of monochromaticity and directivity of electron and radiation fluxes as well as at attaining the controllability of their parameters. The passage of substantial electron currents through laser targets is impossible without the generation of a 'cold' countercurrent, which compensates for the intrinsic magnetic field of the beam. In continuous targets, the presence of the countercurrent results in the instability and filamentation of the relativistic current and its transit to a turbulent regime [2]. In structured targets consisting, for instance, of parallel nanometre fibres, this process is hindered, because the filament parameters are defined by the fibre diameters. One would therefore expect the suppression of the instability, a significant lengthening of the REB free path, and efficient generation of quasimonochromatic hard radiation.

A.A. Andreev Federal State Unitary Enterprise Scientific and Industrial Corporation 'Vavilov State Optical Institute', Birzhevaya ul. 12, 199034 St. Petersburg, Russia; ITMO University, Kronverkskii prosp. 49, 197101 St. Petersburg, Russia; Saint Petersburg State University, Universitetskaya nab. 7–9, 199034 St. Petersburg, Russia;
K.Yu. Platonov Federal State Unitary Enterprise Scientific and Industrial Corporation 'Vavilov State Optical Institute', Birzhevaya ul. 12, 199034 St. Petersburg, Russia; Peter the Great St. Petersburg Polytechnic University, ul. Politekhnicheskaya 29, 195251 St. Petersburg, Russia; e-mail: konstantin_platonov@yahoo.com

Received 28 October 2015
Kvantovaya Elektronika **46** (2) 109–118 (2016)
Translated by E.N. Ragozin

Modern technologies permit making targets in the form of a bundle of fibres of nanometre diameter [3]; the prepulse radiation may leave these fibres intact due to a high contrast ratio of laser radiation. In the course of propagation along the fibre, relativistic electrons execute transverse (betatron) oscillations relative to the fibre axis and generate hard radiation. A similar radiation is generated in the electron oscillations in the ion channel of a transparent plasma [4]. In particular, for a small amplitude of the electron oscillations relative to the channel axis, the characteristic radiation frequency $\omega_{ch} = \omega_p \gamma^{3/2}\sqrt{2}$, where γ is the Lorentz factor of the relativistic electron beam and ω_p is the electron plasma frequency of the background plasma in the channel. In this case, the electron deviation angle from the channel axis when describing the trajectory is smaller than the characteristic radiation divergence angle $\theta \approx 1/\gamma$ (the smallness condition of the oscillation amplitude). When betatron oscillation amplitude r_{max} becomes substantial, i.e. the parameter $K = 1.33\times10^{-10}\sqrt{\gamma n_{ch}}\, r_{max} > 1$ (n_{ch} is the fast electron density in the channel in units of cm^{-3}, r_{max} is taken in μm), the generation of high-frequency harmonics sets in. The characteristic radiation divergence angle increases up to $\theta \approx K/\gamma$, the radiation spectrum becomes quasi-continuous and resembles the synchrotron radiation spectrum. The characteristic energy (which defines the spectrum maximum) assumes a value $\hbar\omega_c \approx 5\times10^{-24}\gamma^2 n_{ch} r_{max}$ (n_{ch} is taken in units of cm^{-3}, r_{max} in μm and $\hbar\omega_c$ in keV). The spectrum amplitude increases proportionally to $\omega^{2/3}$ for frequencies $\omega < \omega_0$, reaches its maximum at $\omega \approx 0.3\omega_c$, and then decays exponentially. The electron synchrotron radiation spectrum in the plasma channel was experimentally observed in Ref. [5]. The coherent nature of the electron betatron radiation in the channel is borne out by the fact that the electron radiation power is proportional to the squared density of the background plasma in the channel. This fact was also confirmed experimentally in Ref. [5].

The mechanism of betatron radiation generation by electrons travelling along the laser target fibres is similar to that in a plasma channel. In both cases, the radiation is generated by the transverse oscillations of relativistic electrons in the electrostatic field of the form of a potential well. However, the betatron fibre radiation offers several advantages over the betatron channel radiation. The first of them is the large number of radiating electrons. The characteristic fast electron density n_{ch} in the channel ranges up to $\sim10^{19}$ cm^{-3}. Electrons are completely extracted from a fibre of radius R by a laser field intensity $E_L > 2eZn_iR$, where e is the electron charge and Z is the average charge of plasma ions with a density n_i. The dimensionless amplitude corresponding to this field $a_L = eE_L/(m_e\omega_L c) \geqslant n_e R/(n_{cr}\lambda_L)$, where m_e is the electron mass, ω_L and λ_L are the central frequency and its corresponding wave-

length of laser radiation, n_e is the electron density and n_{cr} is the critical electron density. For instance, with a field $a_L = 5$ (an intensity of 3.5×10^{19} W cm^{-2}) it is possible to completely extract electrons from a carbon fibre ~10 nm in diameter. A fibre of greater radius will retain a part of electrons and will acquire a charge $\rho \approx E_L R/2$ per unit length under the action of the laser field. In this case, the electrons extracted from the fibre will not be able to move far away from the fibre (this would entail an increase in ρ and the attraction of electrons back to the fibre). The characteristic electron–fibre distance (the Debye radius r_D) is equal to ~1 μm. In this case, the density of 'hot' electrons about the fibre $n_{ch} = Zn_i(R/r_D)^2$. For a carbon fibre 60 nm in diameter, it is equal to 3.2×10^{20} cm^{-3}, which is higher than the electron density in the plasma channel. For a spacing $b \approx 2r_D$ of the target fibres, the laser beam cross section will be filled with fast electrons with a density exceeding the channel electron density.

The second advantage of the fibres is their higher electrostatic field. The field in the electron trajectory in the channel is equal to about $2en_{ch}r_{max}$. In the case of a carbon fibre, the characteristic field in the electron orbit $2\rho/r_D \approx E_L R/r_D \approx 2eZn_i R^2/r_D$, and for $r_{max} \approx 2$ μm it turns out to be approximately 16 times higher than the channel field. The higher field results in a stronger transverse electron acceleration and a higher betatron radiation intensity. In the electron motion in the field of two forces (the electromagnetic wave and the fibre field), a resonance may take place, whereby the electron oscillation energy and the betatron radiation intensity become higher. We emphasise that both target versions are intended for the generation of coherent hard radiation in a preselected and relatively narrow photon energy interval. To efficiently generate hard radiation throughout the possible photon energy range, it is more expedient to direct the photon flux from the fibre target to a continuous solid domain (for instance, by placing the fibre target on a substrate) to obtain the Bethe–Heitler electron bremsstrahlung in the continuous medium. In this case, the spectral intensity depends slightly on the photon energy up to energies comparable to the radiating electron energy. We now turn to the investigation of betatron radiation from nanofibre targets.

2. Numerical simulations

The interaction of laser radiation with nanofibre targets was investigated using two-dimensional particle-in-cell simulations of plasma particle motion. A modified code [6] was employed to simulate the interaction of laser radiation with targets consisting of parallel fibres. The laser radiation with a wavelength λ_L=0.8 μm was incident on the fibre ends along the fibre surfaces. The laser beam diameter was $d_L = 4$ μm, the Gaussian pulse duration was $t_L = 45$ fs and the peak radiation intensity was $I_L = 3\times10^{19}$ W cm^{-2}. The simulations were made in a box measuring 100×100 μm with 25×10^6 cells, the maximum number of quasiparticles in a cell was equal to 30. The targets consisted of carbon fibres of radius $r_w > 30$ nm spaced at intervals $b > 100$ nm. Varying the diameter $d_w = 2r_w$ and spacing b led to the following conclusion [7]. Optimal (in the number and energy of accelerated electrons) among parallel fibre targets are the targets with fibre diameter of the order of the skin layer thickness l_s for a relativistically intense laser field (~40 nm for a $C^{6+}H^{1+}$ hydrocarbon fibre with an initial density of 4×10^{22} cm^{-3}) and an interfibre spacing of the order of the Debye radius for hot electrons ($r_D \approx 1$ μm). These optimal targets completely absorb the laser radiation over a distance of several micrometres from the input fibre ends and convert it to the directional electron flux motion along the fibres. The absorption length depends on the interfibre spacing and may be increased to several hundred micrometres for a spacing exceeding $2\lambda_L$. Figure 1 shows the spatial distribution of fast (the longitudinal momentum $p_z > 1$) electrons travelling in the target with a fibre radius of 30 nm and an interfibre spacing of 1200 nm. The angular and energy distributions of these electrons are depicted in Fig. 2.

The physical reason that permits the fast electrons to travel along the fibres is the occurrence of the counterflow of cold electrons in the fibres: the fast electrons escape from the fibre to give rise to its positive charge, and this charge attracts cold electrons from remote parts of the fibre. That is why the number of fast electrons persists in the propagation through a distance of several tens of micrometres. The counterflow density in the fibre exceeds the fast-electron current density in it (as this takes place, the total currents are approximately

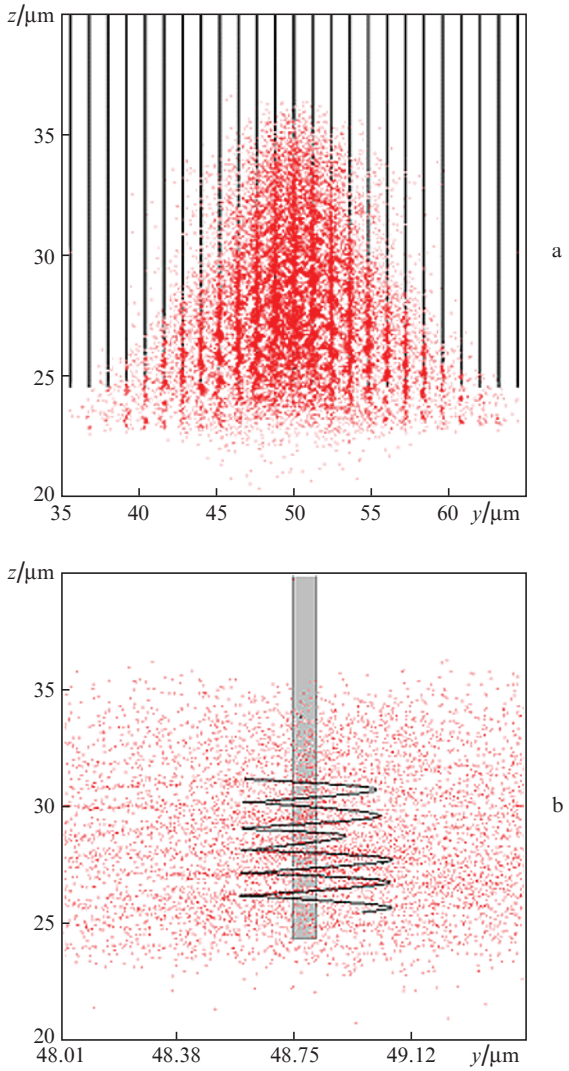

Figure 1. (colour online) Spatial distribution of hot electrons ($p_z > 1$) in carbon fibres 60 nm in diameter (points) at normal (a) and enlarged (b) scales. The vertical lines in Fig. 1a and the grey stripe in Fig. 1b show the ion core of the fibre. The black line in Fig. 1b indicates the electron trajectory derived from Eqns (1). The interfibre spacing is $b = 1200$ nm, the laser beam diameter is $d_L = 4$ μm, the duration is $t_L = 45$ fs and the intensity is $I_L = 3\times10^{19}$ W cm^{-2}.

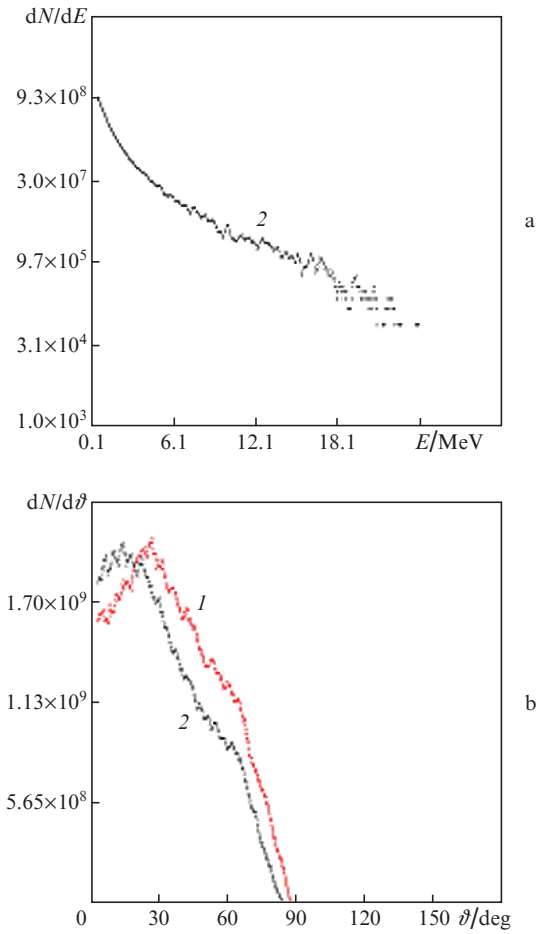

Figure 2. Electron distribution function dN/dE in the fibres for $t = 128$ fs (a) and fast-electron angular distribution for $t = 85$ (*1*) and 128 fs (*2*) (b). The pulse and target parameters are given in the caption to Fig. 1.

equal if account is taken of the fast-electron motion in the vacuum gap between the fibres). As a result, a magnetic field is induced about the fibre, whose polarity is opposite to that of the current of fast electrons themselves. The thus polarised magnetic field cancels the effect of fast-electron current cut-off, which takes place in a continuous target. That is why a bunch of fast electrons is capable of propagating considerable distances along the fibre. In the propagation along the fibre, the main contribution to the electron energy loss and the formation of electron free path is made by the collective bunch-driven ionisation of the target material, which occurs due to the induced counterflow. As shown in Ref. [7], the electron bunch free path along the parallel target fibres amounts to ~1.5 mm, individual fast electrons propagating centimetre-long distances through the now-'neutral' fibre material [8].

An analysis of the fast-electron energy distribution in Fig. 2b suggests that its maximum falls on angles of ~10°. Consequently, in the propagation of electrons along the fibre at nearly the velocity of light there occur their transverse oscillations (a three-dimensional helical motion) in the electrostatic fibre field and a travelling-bunch Debye 'coat' is formed about the fibre. One can also see in Fig. 2b that the characteristic electron propagation angle ($\vartheta = 10°-15°$) sets in after the cessation of the laser pulse [curve (*2*)]. During the course of the pulse, the angle of propagation $\vartheta \approx 30°$ [curve (*1*)]. Therefore, the form of transverse electron oscillations in the fibre vicinity changes upon cessation of the action of the laser field. Figure 1 shows the electron 'coat' (points) surrounding every fibre. An individual fibre with electrons oscillating about it is shown on an enlarged scale in Fig. 1b.

The betatron electron oscillations in the fibre vicinity shown in Fig. 1 generate hard radiation, whose intensity is determined in Section 3. As is evident from Fig. 2a, the characteristic Lorentz factor of electrons $\langle\gamma\rangle \approx 20$ (an energy of ~10 MeV), and in Fig. 2b the electron deviation angle at the peak of distribution $\vartheta \approx 15°$, or 0.25 rad. The corresponding divergence angle $\theta \approx 1/\langle\gamma\rangle$ of relativistic electron radiation is smaller than the characteristic deviation angle of the trajectory (in this case, $K > 1$), and the betatron radiation in its parameters is close to synchrotron radiation for the corresponding radius of curvature of electron trajectory.

3. Analytical model of betatron oscillation generation

3.1. Excitation of transverse electron in-fibre oscillations by external laser field

The electron oscillation amplitude and the fibre charge density are formed during the action of the laser field due to electron extraction to the vacuum gaps between the fibres. At first we consider the electron motion in a fibre portion where the incident laser pulse is slightly distorted (the lower rectangle in Fig. 3a). These are the first 5 μm (this fibre portion depends on the interfibre spacing and may be lengthened) for the PIC simulation performed here. Further along the target (the upper rectangle in Fig. 3a and the rectangle in Fig. 3b) there occurs scattering and absorption of the initial field. In this domain, the field is even higher, but now it is described by the self-consistent solution of the Maxwell equations with the inclusion of electron current. This domain is considered in the subsequent Sections. In the domain that lies even higher the electron motion proceeds only in the electrostatic field of the fibres, and the laser radiation is absent. In this case, the fibre charge is formed self-consistently and depends on the number of fast electrons and, consequently, on the intensity and duration of the laser pulse. In the model of electron motion in the fibre field described below, the fibre charge is a free parameter estimated proceeding from the condition that the model and numerical data must coincide. This approach permits considering the electron motion in a one-particle approximation and calculating the betatron radiation intensity from the calculated trajectory of electron motion.

The equations of electron motion in the vacuum laser field and electrostatic potential of charged fibres (the lower rectangle in Fig. 3a) in a cylindrical system of coordinates are of the form:

$$\frac{\mathrm{d}p_r}{\mathrm{d}\xi} = -\frac{\gamma}{\gamma - p_z}\frac{\partial\tilde{U}(\tilde{r})}{\partial\tilde{r}},$$

$$\frac{\mathrm{d}\tilde{M}_z}{\mathrm{d}\xi} = \frac{\gamma a(\xi)}{\gamma - p_z} \times \frac{[p_r + a(\xi)\cos\varphi]\sin\varphi + [\tilde{M}_z/\tilde{r} - a(\xi)\sin\varphi]\cos\varphi}{1 + \tilde{U}(0) - \tilde{U}(\tilde{r})},$$

$$p_z = \{1 + [p_r + a(\xi)\cos\varphi]^2 + [\tilde{M}_z/\tilde{r} - a(\xi)\sin\varphi]^2 - [1 + \tilde{U}(0) - \tilde{U}(\tilde{r})]^2\}\{2[1 + \tilde{U}(0) - \tilde{U}(\tilde{r})]\}^{-1},$$

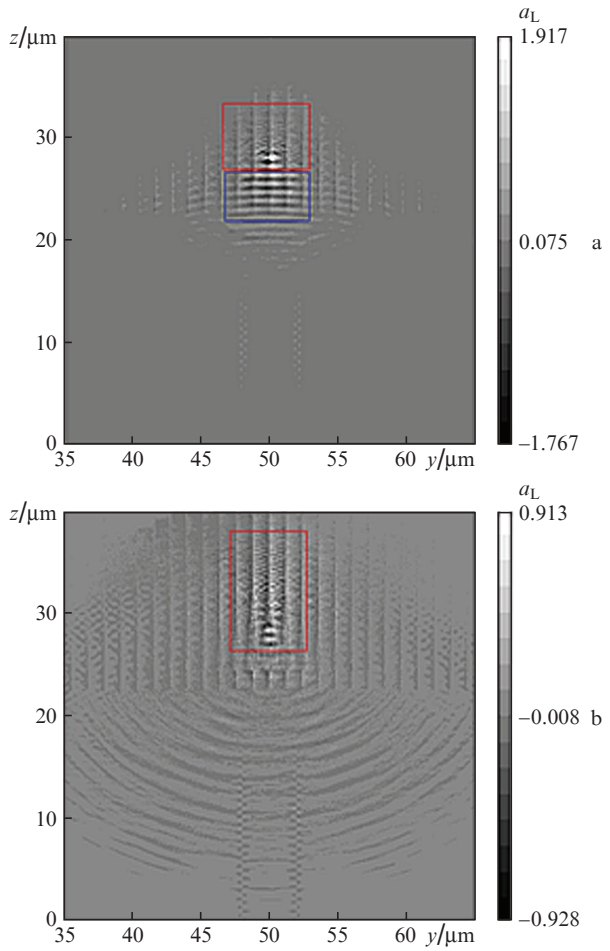

Figure 3. (colour online) Laser field inside the fibre target for $t = 64$ (a) and 85 fs (b). The pulse and target parameters are indicated in the caption to Fig. 1.

$$\frac{d\varphi}{d\xi} = \frac{\tilde{M}_z/\tilde{r} - a(\xi)\sin\varphi}{\tilde{r}(\gamma - p_z)},$$

$$\frac{d\tilde{r}}{d\xi} = \frac{p_r + a(\xi)\cos\varphi}{\gamma - p_z}, \qquad (1)$$

$$\frac{d\tilde{z}}{d\xi} = \frac{p_z}{\gamma - p_z},$$

$$\frac{d\tau}{d\xi} = \frac{\gamma}{\gamma - p_z},$$

$$a(\xi) = a_L \sin\xi, \quad \gamma = p_z + 1 + \tilde{U}(0) - \tilde{U}(\tilde{r}).$$

Here, we introduced the following dimensionless quantities: coordinates $\tilde{r} = \omega_L r/c$, $\tilde{z} = \omega_L z/c$, $\xi = \omega_L(t - z/c)$, $\tau = \omega_L t$; momenta $p_{r,z}$ (in units of $m_e c$); angular momentum $\tilde{M}_z$ (in units of $m_e c^2/\omega_L$), and potential $\tilde{U} = U/(m_e c^2)$. The laser field a_L is linearly polarised along the x axis (in the plane $\varphi = 0$), φ is the azimuthal angle. The potential $\tilde{U}(r)$ of N charged fibres (the fibres are located in the xz plane and aligned with the z axis) is defined by the formula

$$\tilde{U}(r) = \sum_{n=-N}^{N} \frac{1}{m_e c^2} \begin{cases} 2e\rho \ln\dfrac{|\boldsymbol{r} - nb\boldsymbol{e}_x|}{r_w} \text{ at } |\boldsymbol{r} - nb\boldsymbol{e}_x| > r_w, \\ e\rho\left(\dfrac{|\boldsymbol{r} - nb\boldsymbol{e}_x|^2}{r_w^2} - 1\right) \text{ at } |\boldsymbol{r} - nb\boldsymbol{e}_x| < r_w. \end{cases} \qquad (2)$$

Since the PIC numerical simulation was performed in the planar two-dimensional (2D) approximation, a comparison of the solutions of system (1) with the data of numerical calculations is correct when the electron trajectory is planar. Accordingly, to compare with the PIC simulation data, Eqns (1) will be solved numerically in the xz plane, assuming that the electron angular momentum $\tilde{M}_z = 0$ and the angle $\varphi = 0$ in the course of electron motion. This limiting case is correct when the laser wave is linearly polarised. The main forces act on an electron in the polarisation plane xz of the electromagnetic wave, while the motion in the y axis is due to the initial conditions and proceeds at nonrelativistic velocities. We also note that the fibres potential (2) corresponds to the real three-dimensional (3D) geometry, and that to compare with the data of numerical simulations in the 2D limit it would be well to use the potential of planes in lieu of the potential of the fibres (a linear function in lieu of a logarithmic one). Numerical integration of expression (2) with logarithmic and linear potentials (with the same depth and width of the potential well for the electron) showed that the main characteristics of electron motion for these potentials coincide to within a factor of the order of unity. That is why, below, the potential (2) will also be used in the comparison of the results of model and numerical calculations.

The radiation power of the electron travelling in the xz plane is calculated from the solution of the system (1):

$$\frac{P_{1e}}{P_0} = \tilde{P}_{1e} = \gamma^4(w_r^2 + w_z^2) + \gamma^6(w_r v_r + w_z v_z)^2,$$

$$P_0 = \frac{2e^2\omega_L^2}{3c}, \qquad (3)$$

where the components of dimensionless electron velocity v and acceleration w are determined from Eqns (1) as

$$v_r = \frac{d\tilde{r}}{d\tau}, \quad v_z = \frac{d\tilde{z}}{d\tau},$$

$$w_r = \frac{1 - v_z}{\gamma}\frac{\partial a(\xi)}{\partial\xi} + \frac{\partial\tilde{U}(\tilde{r})}{\gamma\partial\tilde{r}} - \frac{v_r^2}{\gamma}\left[\frac{\partial\tilde{U}(\tilde{r})}{\partial\tilde{r}} + \frac{\partial a(\xi)}{\partial\xi}\right], \qquad (4)$$

$$w_z = \frac{v_r}{\gamma}\frac{\partial a(\xi)}{\partial\xi}.$$

We note that the main contribution for the thin fibres under consideration is made by the upper term in expression (1), while in plasma channels, by contrast, the lower term is significant.

The system of equations (1) can be solved only numerically. It is convenient to introduce the dimensionless fibre charge density $\beta = 2e\rho/(m_e c^2)$ and plot the time dependences of the Lorentz factor γ and the Lorentz factor γ_z of longitudinal electron motion for different β (Fig. 4). The electron trajectory calculated using Eqns (1) (the black line in Fig. 1b) coincides with the trajectory obtained by PIC simulations (the crowdings of points in Fig. 1b) for parameter $\beta = 0.23$, which corresponds to the extraction of 8% of the electron charge from the fibre.

As is clear from Fig. 4b, a substantial increase in the electron oscillation energy and betatron radiation intensity are possible for a fixed laser pulse intensity and a variation of the fibre charge density (for $\beta = 0.19$). This case calls for a fine adjustment of fibre and laser pulse parameters will be dis-

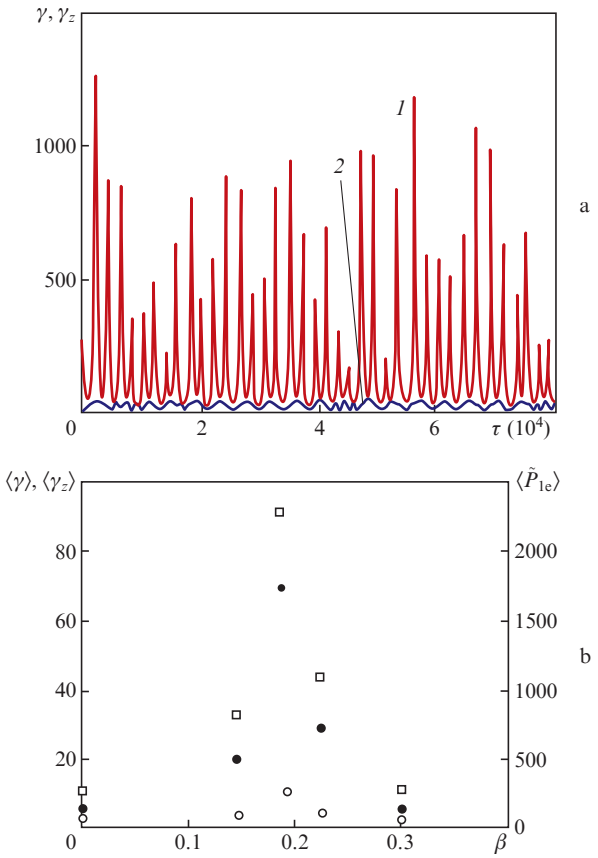

Figure 4. (colour online) Time dependences of the Lorentz factor γ (*1*) and the longitudinal Lorentz factor γ_z (*2*) for an electron in fibre of radius 30 nm for $a_L = 5$ and $\beta = 0.19$ (a) as well as time-averaged values of $\langle\gamma\rangle$ (□), $\langle\gamma_z\rangle$ (○), and the dimensionless radiation power $\langle\tilde{P}_{1e}\rangle$ (●) as functions of the dimensionless fibre charge density β (b). The value $\tau = 2\times10^4$ corresponds to a dimensional time of 8.5 ps.

cussed in Section 5 of the present paper, and in Section 3.2 we determine the betatron radiation intensity outside the resonance domain.

3.2. Intensity of the betatron radiation of electrons in their propagation along the fibre

Formula (3) permits determining numerically the intensity of betatron radiation for a single electron by numerical solution of equations of motion (1) as well. Obtaining analytical results calls, first of all, for simplifying the system of the equations of motion. The data of PIC simulation presented in Fig. 3 suggest that the weakly distorted 'vacuum' transverse laser field occupies the first ~5 μm of the fibre, the next ~5 μm are occupied by the transition domain, where the transverse field is strongly distorted and lower in amplitude. Further (after the first ~10 μm) electrons travel along the fibre in its ambipolar field without the effect of transverse fields on electron dynamics. The angular and energy electron distributions formed by that time are depicted in Fig. 2 [curves (*2*)]. The angular electron distribution upon cessation of the action of the laser field [Fig. 2b, curve (*2*)] peaks at a smaller angle than in the case when the electron was travelling in the wave field and the fibre field [Fig. 2b, curve (*1*)]. Therefore, on exiting the domain of laser pulse action (on its cessation), the transverse electron oscillations relax partly because one of the forces disappears. We consider analytically the radiation generation in the domain where the transverse field is nonexistent and the electrons oscillate only in the potential fibre field. In Fig. 1, this corresponds to distances of ~10 μm and further from the fibre front end. The angular and energy electron distribution function f_e is assumed to be known from numerical simulations (see Fig. 2).

To analytically calculate the radiation power of an electron bunch with a known distribution function (Fig. 2) travelling along the fibre beyond the domain of laser field penetration, use is made of formula [9]

$$P(t) = \int \frac{2e^2}{3c^2}\,\frac{w(t,r_0,p_0)^2 - [\boldsymbol{w}(t,r_0,p_0)\boldsymbol{v}(t,r_0,p_0)]^2/c^2}{[1-v(t,r_0,p_0)^2/c^2]^3} \times f_e(r_0,p_0)\,\mathrm{d}^3r_0\,\mathrm{d}^3p_0. \tag{5}$$

Formula (5) gives the radiation power (3) of a single electron averaged over the electron distribution. Performing calculations by formula (5) necessitates the trajectory of motion of an individual electron for given initial conditions $\boldsymbol{r}(t,r_0,p_0)$. The trajectory of motion follows from system (1), in which the laser field is absent and the fibre potential (2) remains the same. The fibre charge beyond the domain of the laser field action is defined by formula (2) as before, because the number of fast electrons persists in the bunch propagating through a distance of several tens of micrometres. As shown in Ref. [10], the fibre charge induced due to the redistribution of cold electrons is equal to the charge of hot electrons travelling above the fibre surface. In the absence of the laser field, system (1) is solved analytically. Conserved in the field of every fibre are the momentum p_z, angular momentum $\tilde{M}_z$, and the total energy of an individual electron oscillating in this field with a dimensionless amplitude $\tilde{r}_{max}$:

$$\frac{\sqrt{1+p_z^2+\tilde{M}_z^2/\tilde{r}^2}}{\gamma_z\sqrt{1-\dot{\tilde{r}}/c^2}} + \frac{\beta}{\gamma_z}\ln\frac{\tilde{r}}{\tilde{r}_{max}} = 1, \qquad \gamma_z = \sqrt{1+p_z^2+\tilde{M}_z^2/\tilde{r}_{max}^2}\,. \tag{6}$$

From expressions (6) we obtain the analytical description of transverse electron oscillations and longitudinal electron motion:

$$\tau = \int \mathrm{d}\tilde{r}\left(1-\frac{\beta}{\gamma_z}\ln\frac{\tilde{r}}{\tilde{r}_{max}}\right) \times\left[\left(1-\frac{\beta}{\gamma_z}\ln\frac{\tilde{r}}{\tilde{r}_{max}}\right)^2 - 1 - \frac{\tilde{M}_z^2(\tilde{r}_{max}^2/\tilde{r}^2-1)}{\tilde{r}_{max}^2\gamma_z^2}\right]^{-1/2},$$
$$\dot{\tilde{z}} = \sqrt{1-\dot{\tilde{r}}^2}\,\frac{p_z}{\sqrt{1+p_z^2+\tilde{M}_z^2/\tilde{r}^2}}, \qquad \dot{\varphi} = \frac{\tilde{M}_z}{\tilde{r}^2}\left(\frac{1-\dot{\tilde{r}}^2}{1+p_z^2+\tilde{M}_z^2/\tilde{r}^2}\right)^{1/2}. \tag{7}$$

The radial oscillation period T follows from expressions (7) and is described by the expression

$$\frac{cT(\mu,\varepsilon_\varphi)}{r_{max}} = 2\int_{x_1(\mu,\varepsilon_\varphi)}^{1}\mathrm{d}x\,\frac{1-\mu\ln x}{\sqrt{(1-\mu\ln\tilde{x})^2-1-\varepsilon_\varphi^2(\tilde{x}^{-2}-1)}}, \qquad \mu = \frac{\beta}{\gamma_z},\quad \varepsilon_\varphi = \frac{\tilde{M}_z}{\gamma_z r_{max}}, \tag{8}$$

where $\tilde{x} = \omega_L x/c$ and the turning point $\tilde{x}_1$ is defined by the equation $(1-\mu\ln\tilde{x}_1)^2 - \varepsilon_\varphi^2(\tilde{x}_1^{-2}-1) = 1$. The dimensionless parameter μ is the ratio between the characteristic potential energy to the kinetic energy of motion along the fibre and determines the deviation angle of the electron trajectory. The parameter ε_φ is related to the azimuthal motion and is the dimensionless ($\varepsilon_\varphi = v_\varphi/c$) velocity of azimuthal rotation. As mentioned above, in the case of a linearly polarised laser pulse $v_\varphi \ll c$ and the parameter ε_φ is small.

Calculations show that the period is sufficiently accurately described by the expression

$$\frac{cT(\mu,\varepsilon_\varphi)}{r_{\max}} \approx 1.5 + \frac{2}{\sqrt{\mu}}. \tag{9}$$

The characteristic radiation frequency ω^* (which defines the spectral power peak) of a relativistic electron executing radial oscillations of significant amplitude (in Fig. 2b, the electron deviation angle ϑ exceeds the characteristic radiation divergence angle θ) coincides with the characteristic synchrotron radiation frequency [9], provided that in its expression the electron in-fibre oscillation period (9) is substituted for the electron rotation period in the magnetic field:

$$\omega^* = \gamma_z^3 2\pi/T \approx \gamma_z^3 4\pi c/(7r_{\max}). \tag{10}$$

In expression (9) the parameter $\mu \approx 1$, because the electron deviation angle in Fig. 2b is sufficiently large. The explicit form of the frequency dependence of the spectral power is given by formula (19) below. The individual electron radiation power [the integrand in expression (5)] is obtained on substitution of the electron acceleration (4) in expression (5). As a result, the power of radiation by an individual electron is expressed in terms of its transverse coordinate:

$$P_{1e}(r) = \frac{8e^4\rho^2\gamma_z^2}{3m_e^2c^3}\frac{[1+\varepsilon_\varphi^2(r_{\max}^2/r^2-1)]}{r^2}. \tag{11}$$

The time dependence of the power is obtained by substituting in formula (11) the radial motion law $r(t)$, which is defined by the first expression in formulas (7). The emergence of r^{-2} in formula (11) is readily explainable: since the fibre field is $\propto 1/r$, the acceleration is also $\propto 1/r$, and the power is proportional to the square of the acceleration, i.e. to $1/r^2$. For $r = 0$, the fibre field, the acceleration, and the power formally turn to infinity. That is why in the absence of the angular momentum ε_φ the radius r [and the lower limit of integration in expression (7)] should be limited by the fibre radius r_w. When the angular momentum is nonzero, the electron cannot fall at point $r = 0$ and formula (11) always gives a finite power value.

The expression for the radiation power of an individual electron averaged over the oscillation period is obtained by the time averaging formula (11), and after a change of integration variable takes on the form

$$\langle P_{1e}\rangle = \frac{1}{T}\int_0^T P_{1e}(t)\,dt = \frac{2}{T}\int_{r_{\min}}^{r_{\max}} P_{1e}(r)\frac{dr}{\dot{r}(r)}$$

$$= \frac{2e^2c\gamma_z^4}{3r_0^2}\,g(\mu,\varepsilon_\varphi), \tag{12}$$

where the function

$$g(\mu,\varepsilon_\varphi) = \mu^2\int_{x_1(\mu,\varepsilon_\varphi)}^1 \frac{(1-\mu\ln\tilde{x})[1+\varepsilon_\varphi^2(\tilde{x}^{-2}-1)]}{\tilde{x}^2\sqrt{(1-\mu\ln\tilde{x})^2 - 1 - \varepsilon_\varphi^2(\tilde{x}^{-2}-1)}}\,d\tilde{x}$$

$$\times\left[\int_{x_1(\mu,\varepsilon_\varphi)}^1 d\tilde{x}\,\frac{1-\mu\ln\tilde{x}}{\sqrt{(1-\mu\ln\tilde{x})^2 - 1 - \varepsilon_\varphi^2(\tilde{x}^{-2}-1)}}\right]^{-1}. \tag{13}$$

It is plotted in Fig. 5 for different ε_φ. Unlike the oscillation period, the dependence of the time-averaged radiation power on the parameter ε_φ is strong. The growth of the power with a decrease in the electron angular momentum is explained as follows: for small momenta, electrons approach the fibre closer, where the field is stronger, the acceleration is greater and, accordingly, the radiation power is higher. Interestingly, in the electron propagation through an ion channel [see the potential in the lower line in expression (2)], which was considered in Refs [4, 11], the radiation power is defined by the formula similar to formula (11):

$$P_{1e}^{ch}(r) = \frac{8e^4\rho_{ch}^2\gamma_z^2}{3m_e^2c^3}\frac{[1+\varepsilon_\varphi^2(r_0^2/r^2-1)]r^2}{r_{ch}^4}, \tag{14}$$

where ρ_{ch} and r_{ch} are the channel charge per unit length and the channel radius. By comparing expressions (11) and (14), one can see that the ratio between the radiation powers in the channel and the fibre is defined by the ratio between ρ_{ch}/r_{ch} and ρ/r_w, or between $n_i^{ch}r_{ch}$ and $n_i r_w$. For a channel of radius 3 μm (equal to the radius of the laser beam) in the plasma with a density of 10^{19} cm^{-3} and for a fibre of radius 30 nm with an ion density of 6×10^{22} cm^{-3}, the radiation power of one electron in the fibre exceeds that in the channel by a factor of ~50.

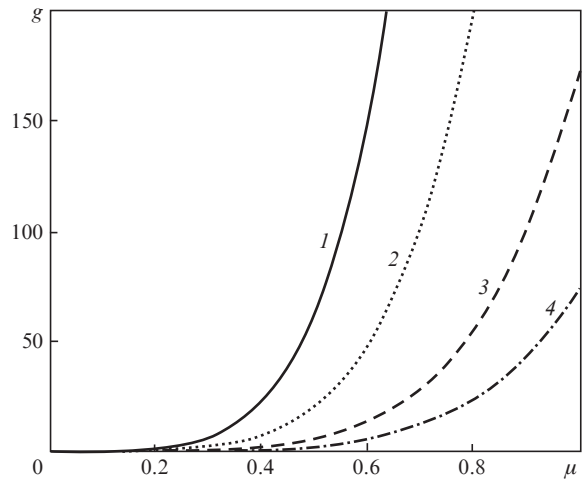

Figure 5. Dependences $g(\mu)$ for ε_φ = 0.05 (*1*), 0.1 (*2*), 0.2 (*3*), and 0.3 (*4*).

Formula (12) defines the radiation power of an individual electron. The electron radiation power for all fibres is obtained, according to expression (5), by averaging formula (12) over the distribution function (Fig. 2). The electron angular and energy distributions ($\tan^2\vartheta = \mu$, γ_z) for all target fibres are depicted in Fig. 2. The radiation power averaged over the electron distribution $f_e(\mu,\gamma_z)$ is defined by the expression

$$\langle P\rangle = \int f_e(\mu,\gamma_z)\,d\mu\,d\gamma_z \frac{2e^2 c\gamma_z^4}{3r_0^2}\, g(\mu,\varepsilon_\varphi). \quad (15)$$

Numerical calculation by formula (15) for a small dimensionless value ($\varepsilon_\varphi = 0.1$) of the electron angular momentum gives $\langle P\rangle = 2.7\times10^{12}$ erg s^{-1} ($\varepsilon_\varphi = 0.1$ corresponds to the approximate equality between the azimuthal and characteristic radial velocities). For an intensity $I_L = 3\times10^{19}$ W cm^{-2} and $d_L = 4$ μm, the laser power P_L is equal to 5×10^{19} erg s^{-1}. The power conversion coefficient $\varepsilon_P = 0.8\times10^{-6}$. For a channel with an electron density of 10^{19} cm^{-3}, the coefficient ε_P is approximately 200 times lower. Therefore, outside the domain of the laser field action the conversion coefficient is low (lower than, for instance, the coefficient of conversion to the characteristic radiation of target ions), and this case is nonoptimal for the efficient generation of coherent hard radiation.

4. Resonance betatron oscillations

In the electron motion through a fibre target, a resonance may occur between the electron oscillations in the field of the laser wave and in the electrostatic fibre field. The resonance was observed for $\beta = 0.19$ in the analytical model above (Fig. 4b). The amplitude (energy) of betatron oscillations increases under resonance conditions (see Fig. 4b), and it is precisely the resonance case that holds the greatest interest for research and is optimal for increasing the power of secondary radiation. The betatron electron oscillations under the conditions being considered are characterised by a strong nonlinearity (the amplitude dependence of the frequency), and therefore a numerical search for the resonance parameters of the target and the laser pulse calls for the variation over wide limits of at least of one of these parameters.

To find the resonance conditions, we modelled the interaction of the laser pulse (its parameters are given above) with one fibre of varying diameter, $d_w = 5$–100 nm, over a distance of 75 μm. On reaching $d_w = 13$ nm (at a point $z = 35$ μm) there occurred a substantial (approximately four-fold) increase in transverse electron momentum and electron energy. To verify the resonance diameter value, simulations were made of targets with fibre diameters of 7 and 13 nm and an interfibre spacing of 1200 nm. The laser pulse parameters are the same as in Fig. 1. Figure 6 shows the dependence of the highest electron γ factor on the dimensionless fibre charge density β. The fibre charge density was determined from the difference of average electron and ion densities inside the fibre and was equal to 0.06 and 0.08 for $d_w = 7$ and 13 nm, respectively. Given additionally in Fig. 6 are the above simulation data for $d_w = 60$ nm ($\beta = 0.23$) and the maximal electron Lorentz factor in the field of a laser wave of intensity 3×10^{19} W cm^{-2} in the absence of fibres. A comparison of numerical data (Fig. 6) with the analytical model (Fig. 4b) suggests that a clearly pronounced resonance is observed in the numerical simulation, like in the model, however for $\beta \approx 0.08$. The discrepancy (by about a factor of two) between the resonance charge value obtained in the analytical model and numerical simulation data is due to the approximations assumed: in the mode, β is an independent parameter, while in the simulations it is settled in a self-consistent way and is determined by the pulse and target parameters.

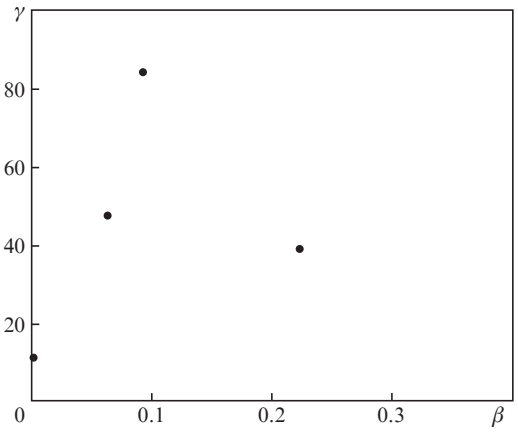

Figure 6. Dependence of the maximal electron γ factor on the dimensionless fibre charge density β, which was obtained from 2D PIC simulation data. The laser pulse parameters are the same as in Fig. 1.

The resonance value $\beta = 0.19$ of the analytical model corresponds to complete extraction of electrons from a fibre ~3 nm in diameter (or, for a fibre of larger diameter, to a partial extraction proportionally to the area ratio). In the numerical simulation, the resonance diameter was equal to 13 nm and the extraction of electrons was partial. In the analytical model, the average electron energy at resonance is approximately two times higher (like in the numerical simulation) and the average radiation intensity is approximately four times higher in comparison with the non-resonance case ($\beta = 0.23$). Unlike the electron motion in the wave field (without a fibre, $\beta = 0$) there occurs a more significant increase in radiation energy (eight-fold) and power (60-fold).

The analytical model permits studying the properties of resonance with fibre diameter variation (see Fig. 4). In the model calculations, the resonance is inherently 'sharp': for instance, the values $\beta = 0.18$, 0.19, and 0.2 result in several-fold different electron energies and radiation intensities. In a real experiment and in the numerical simulation, the values of r_w and a_L determine the charge density, because it is formed in a self-consistent way. Accordingly, in the model the parameter β may not be arbitrarily selected. We estimate it from the condition that the electrostatic fibre field, which appears due to the extraction of electrons by the laser field, has to be comparable to the laser field: $2e\rho/r_w = 2e(n_i - n_e)r_w \approx E_L$. From this relationship it follows that $\beta \approx a_L r_w \omega_L/c$. For $r_w = 30$ nm and $a_L = 5$, the model value $\beta \approx 1.2$, which is greater than the simulation resonance value $\beta = 0.19$, because the model does not permit determining the corresponding parameter exactly for a partial electron extraction from the fibre. However, it permits determining the interval for the search of the resonance fibre diameter for given laser parameters. The resonance is sensitive to the temporal profile of the laser pulse. Replacing a rectangular pulse envelope (Fig. 4) with a Gaussian profile for $\beta = 0.19$ results in a lowering of the resonance values in Fig. 4b by about a factor of two. However, the resonance itself persists for a smooth profile as well.

Interestingly, in the variation of laser target thickness the energy of fast electrons shows a maximum for a certain value of the thickness [12]. However, for a fibre target this maximum is sharper and is interpreted as a consequence of the resonance in electron oscillations.

The resonance condition is analytically written as the resonance condition between the laser pump and the oscillations in the fibre field: $\omega_L = 2\pi/T$. The resonance condition

corresponds to the presence of two independent forces in the equation of radial motion and the absence of coupling between the longitudinal and transverse motions. This case is realised for the system (1) in the limit $p_{y,z} \ll 1$, $\gamma \approx \gamma_z \approx 1$, $a(\xi) \ll 1$, i.e. for low amplitudes of the laser field. In this case, the equation of radial motion assumes the form

$$\ddot{\tilde{r}} = \frac{\partial a(\xi)}{\partial \xi} + \frac{\partial \tilde{U}(\tilde{r})}{\partial \tilde{r}}. \tag{16}$$

For small electron deviations from the fibre axis [see the potential in the lower line of expression (2)] its motion becomes harmonic:

$$\ddot{\tilde{r}} + \beta \tilde{r}_w^{-2} \tilde{r} = a_L \cos\xi. \tag{17}$$

The resonance condition for Eqn (17) is of the form $\beta = \tilde{r}_w^2 = (2\pi r_w/\lambda_L)^2 \ll 1$. With an increase in oscillation amplitude and electron escape from the fibre, the oscillations in the potential well, which are described by expression (16), become nonlinear: the period T depends on the amplitude r_{max},

$$\frac{cT}{r_{max}} \approx 1.5 + \frac{2}{\sqrt{\beta}}. \tag{18}$$

In this case, the resonance condition takes on the form $\tilde{r}_{max}(1.5 + 2\beta^{-1/2}) \approx 2\pi$. We emphasise that the resonance in nonlinear oscillations is different in properties from the resonance in the linear equation (17): as the amplitude increases, the frequency changes and the system goes out of resonance. As this takes place, the amplitude begins to decrease, the frequency returns to the resonance value, and the amplitude begins to grow again. As a result, there occur aperiodic variations of the amplitude and energy of electron oscillations, which can be seen, for instance, in the time dependence of γ in Fig. 4a. In this case, the oscillation amplitude varies aperiodically and remains finite even in the absence of dissipation forces.

For a relativistic amplitude of the laser field ($a(\xi) > 1$), the transverse electron motion mixes with the longitudinal one, and in the complete system (1) it is impossible to single out two separate transverse forces with separate drive frequencies and write the resonance condition in an analytical form. The system (1) permits determining only the trends in the variation of the resonance condition. Specifically, the smallness of the characteristic angle of electron propagation (Fig. 2b) permits putting γ_z = const in the zero approximation, and then the influence of longitudinal motion on the transverse one comes to an increase in effective electron mass and the period of transverse oscillations becomes longer. According to formula (9), the period lengthens with increasing γ_z. As a result, the dimensionless quantity $T\omega_L$ also increases: in the calculation performed by the analytical model, for instance, for resonance parameters $\tilde{r}_{max} \approx 20$, $\langle\gamma_z\rangle \approx 10.6$, and $\beta = 0.19$ we obtain $T\omega_L \approx \tilde{r}_{max}(1.5 + 2\sqrt{\gamma_z/\beta}) \approx 312 \gg 2\pi$. In the plasma channel [4, 11] the situation is similar: at resonance the ratio ω_p^{ch}/ω_L of the oscillation frequency in the channel to the laser frequency is equal to ~0.12.

The fibre charge density β^* optimal for maximising the amplitude $\tilde{r}(\tau)$ is numerically related to a_L as $\beta^*(a_L) \approx 0.02 a_L^{1.3}$, which is true in the interval $2 < a_L < 30$ provided that the interfibre spacing $b > 2\tilde{r}(\tau)$, $\forall\tau$. The resonance parameter in the system (1) depends only slightly on the fibre radius in the range $r_w = 10-200$ nm.

Since β is not an arbitrary parameter in reality but is determined by laser pulse and target parameters, we performed calculations for intensities of 10^{20} and 10^{21} W cm^{-2} to find the optimal fibre diameter as a function of laser intensity. The remaining parameters were the same as in the simulations (see Fig. 1). For each of these two intensities we performed enumeration of the fibre diameters in the 20–200 nm range at 20-nm increments. We selected the diameter for which the electron energy was highest. The results of these calculations are given in Fig. 7 (points). One can see that the dependence of the optimal diameter on the field amplitude is close to the linear one, i.e. $d_w \propto \sqrt{I_L}$. Figure 7 shows the values of fibre charge density β for each of the three optimal diameters for comparing the data of numerical simulations with the optimal dimensionless charge density $\beta^*(a_L)$ which follows from Eqns (1). The dotted curve shows the dependence $\beta^*(a_L)$. One can see that the scaling formula for the optimal charge density is consistent with the data of numerical 2D PIC simulations.

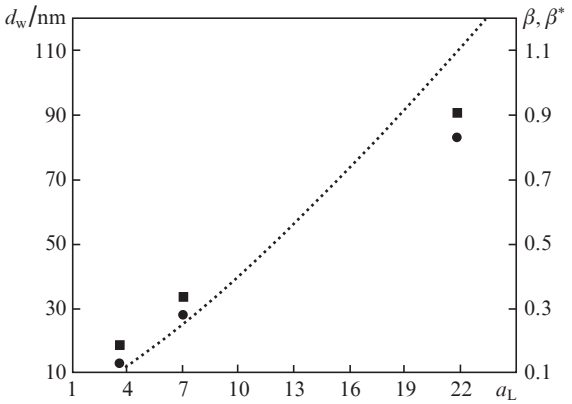

Figure 7. Optimal fibre diameter d_w (●) as well as dimensionless fibre charge densities β (■) and β^* (the curve) as functions of the dimensionless amplitude a_L of the laser field. The duration of laser pulses is equal to 45 fs, the beam diameter is equal to 4 μm, and the target interfibre spacing to 1200 nm.

In the resonance case, the coefficient of laser radiation conversion to coherent X-rays may be substantially improved. To this end, the target fibres must be optimised in diameter and their spacing must be increased to $b \geqslant 2\lambda_L$ for lengthening the laser-pulse penetration depth in the fibre target and effecting the joint propagation of electrons and the laser pulse along the fibres. In Fig. 3a, this corresponds to a larger height of the lower rectangle and the absence of other domains. Analytical formula (15) for the betatron radiation power is invalid in this case (a transverse field is present) and an estimate is made numerically from formulas (1), (3) directly. Since the radiation power rises with increase in a_L, we take the greatest possible experimental value $a_L = 30$ to determine the maximal conversion coefficient. Then, calculations by the formulas of system (1) give the optimal value $\beta^* = 1.7$ for $r_w = 150$ nm. The energy and power of individual electron radiation obtained by formula (3) are as follows: $\langle\gamma\rangle = 14500$, $\langle\tilde{P}_{1e}\rangle = 3\times10^{10}$, $\langle\gamma_z\rangle = 530$ ($\tilde{r}_{max} = 120$).

The resonance value of β defines the number of fast electrons, because $\rho = en_{ch}/(ct_L) = \beta m_e c^2/(2e)$. For an estimate, instead of averaging over the distribution function we multiply the intensity of radiation by an individual electron by n_{ch}. The conversion coefficient ε_P is calculated assuming that the fibre 'intercepts' laser radiation over an effective area πr_{max}^2. Then

$$\varepsilon_P = \frac{n_{ch} P_{1e}}{I_L \pi r_{max}^2} = \frac{4e^2\omega_L^2 t_L}{3m_e c^3} \frac{\beta \tilde{P}_{1e}}{a_L^2 \tilde{r}_{max}}$$

and for $t_L = 30$ fs, $a_L = 30$ we obtain $\varepsilon_P \approx 0.02$.

The maximum of spectral power of the radiation falls on an energy $\hbar\omega_c \approx (\hbar\omega_L \gamma_z^3 \pi/\tilde{r}_{max})[1.5 + 2(\beta/\gamma_z)^{-1/2}]$, which amounts to ~2.45 MeV for our parameters. The peak width is equal to about 1.5 MeV. The form of the spectrum corresponds to the spectrum of synchrotron radiation. We emphasise that the fibre target which corresponds to the resonance condition has a ratio of fibre diameter to the interfibre spacing $d_w/b = 0.02$. As shown in Ref. [7], the highest absorption (the highest total energy of hot electrons) is realised for $d_w/b \approx 0.05$. In this case, the absorption length amounts to a few micrometres. Therefore, maximising the conversion to betatron radiation requires a more 'rarefied' fibre target, in which the laser pulse propagates a distance of several tens of micrometres to give rise to the resonance of electron oscillations in the transverse field and in the potential fibre field.

5. Comparison of the powers of betatron radiation and bremsstrahlung

In the electron motion through a medium, the bremsstrahlung power is defined by the expression

$$P^{BG} = \frac{4e^6 Z^2 n_i \gamma}{m_e c^2 \hbar} \ln(2\gamma),$$

and the betatron-to-bremsstrahlung radiation power ratio

$$\frac{\langle P \rangle}{P^{BG}} = \frac{137 m_e c^2 \gamma_z^4}{6x_0^2 e^2 Z^2 n_i \gamma \ln(2\gamma)} \mu^2.$$

For an intensity of 10^{21} W cm^{-2}, $r_{max} \approx 1$ μm, $\mu \approx 1$, $\gamma_z \approx 6$, $\gamma \approx 36$, $n_i \approx 6\times10^{22}$ cm^{-3}, and $Z = 6$ we obtain $\langle P \rangle/P^{BG} = 0.03$. Therefore, from the standpoint of maximising the number of hard photons it is more advantageous to direct fast electrons into a continuous medium. We note that in the fibre case the main part of the electron trajectory passes outside of the fibre. That is why the power of bremsstrahlung is lower by about a factor r_{max}/r_w (actually even lower, because large impact parameters also contribute to the bremsstrahlung). For $r_{max} \approx 1$ μm and $r_w \approx 50$ nm it is approximately 20 times lower. Then, in the fibre case the bremsstrahlung power is of the order of the betatron radiation power but is lower than the radiation power of the same number of electrons in a continuous medium. After the generation of electrons in the fibre, to maximise the hard radiation yield it is advantageous to direct them into the continuous medium rather than let them travel along the fibre.

The spectral power of betatron radiation is defined by the formula, which is similar to that for synchrotron radiation:

$$\frac{dP_{1e}}{d\omega} = \frac{\sqrt{3}e^2\gamma_z}{2\pi r_0} \mu^2 F\left(\frac{\omega r_0 (1.5 + 2\mu^{-1/2})}{3\pi\gamma_z^3 c}\right), \quad (19)$$

where

$$F(x) = x\int_x^\infty K_{5/3}(\xi)\,d\xi.$$

The peak of expression (19) falls on the frequency $\omega_{cw} \approx (\gamma_z^3 \pi c/r_0)(1.5 + 2\mu^{-1/2})$. Integrating expression (19) over all frequencies gives the total radiation power (12).

The spectral power of Bethe–Heitler radiation

$$\frac{dP^{BG}}{d\omega} = \frac{16e^2 Z^2 n_i}{3m_e^2 c^4} \ln\frac{2\gamma^2 m_e c^2}{\hbar\omega}.$$

The spectral power ratio at the peak point $\omega = \omega_{cw}$

$$\frac{dP/d\omega}{dP^{BG}/d\omega} = \frac{3\sqrt{3}\gamma_z m_e^2 c^4}{32\pi x_0 e^4 Z^2 n_i \ln[4x_0\gamma^2 m_e c/(3\hbar\gamma_z^3)]} \mu^2,$$

which amounts to ~400 for a fibre 30 nm in diameter with an ion density of 6×10^{22} cm^{-3}. Therefore, the peak of betatron radiation towers above the bremsstrahlung background even in the case of a continuous medium. For fibres, the bremsstrahlung background power is lower by r_{max}/r_w times at the most. And so the amplitude of the peak should exceed the bremsstrahlung background by approximately three orders of magnitude.

The betatron radiation of electrons is incoherent over their ensemble, and therefore the passage from the power of individual electron radiation to the power of bunch radiation comes to the averaging over the electron bunch distribution function.

6. Conclusions

A laser target of thin fibres is a source of coherent X-ray betatron radiation similarly to a plasma channel in an optically transparent plasma. For optimal fibre diameters and interfibre spacing, the power of X-ray radiation from the fibre target is two orders of magnitude higher than the power from a plasma channel for the same parameters of the laser pulse. The betatron radiation under consideration is characterised by a high photon energy corresponding to the peak of spectral radiation intensity, coherence in the number of ions per unit fibre length, and the absence of coherence in the number of radiating fast electrons. The existence of resonance in laser intensity and fibre diameter permits attaining an energy efficiency of ~1% in laser-to-coherent X-ray photon conversion at intensities of ~10^{21} W cm^{-2}. The betatron radiation has a small divergence aligned with the fibres and a spectrum coinciding in shape with the spectrum of synchrotron radiation. Therefore, a target in the form of a bundle of thin fibres may be considered as an efficient laser-driven source of coherent X-rays.

References

1. Mourou G., Tajima T., Bulanov S. *Rev. Mod. Phys.*, **78**, 309 (2006).
2. Gibbon P. *Short Pulse Laser Interactions with Matter* (London: Imperial College Press, 2005).

3. Ostrikov K. *Rev. Mod. Phys.*, **77**, 489 (2005).
4. Kostyukov I., Kiselev S., Pukhov A. *Phys. Plasmas*, **10**, 4818 (2003).
5. Nakajima H., Tokita S., et al. *Phys. Rev. Lett*., **110**, 155001 (2013).
6. Kemp A., Ruhl H. *Phys. Plasmas*, **12**, 033105 (2005).
7. Andreev A.A., Platonov K.Yu. *Opt. Spektrosk*., **117**, 298 (2014).
8. Joy D., Luo S. *Scanning*, **11**, 176 (1989).
9. Landau L.D., Lifshits E.M. *The Classical Theory of Fields* (Oxford: Pergamon Press, 1975; Moscow: Nauka, 1973).
10. Andreev A., Ceccotti T., Levy A., Platonov K., Martin Ph. *New J. Phys*., **12**, 045007 (2010).
11. Arefiev A., Khudik V., Schollmeier M. *Phys. Plasmas*, **21**, 033104 (2014).
12. Andreev A.A., Platonov K.Yu., Schnürer M., Prasad R., Ter-Avetisyan S. *Phys. Plasmas*, **20**, 033110 (2013).